

NMR Solution Structure and Condition-Dependent Oligomerization of the Antimicrobial Peptide Human Defensin 5

Andrew J. Wommack,[†] Scott A. Robson,[‡] Yoshitha A. Wanniarachchi,[†] Andrea Wan,[†] Christopher J. Turner,[§] Gerhard Wagner,[‡] and Elizabeth M. Nolan^{*,†}

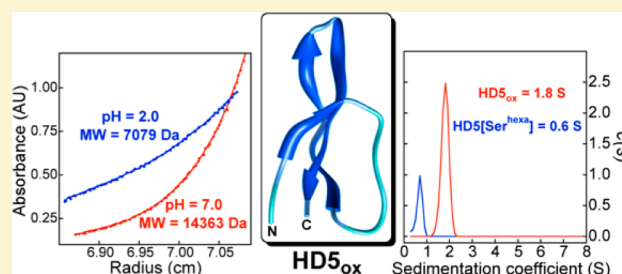
[†]Department of Chemistry, Massachusetts Institute of Technology, Cambridge, Massachusetts 02139, United States

[‡]Department of Biological Chemistry and Molecular Pharmacology, Harvard Medical School, 240 Longwood Avenue, Boston, Massachusetts 02115, United States

[§]Francis Bitter Magnet Laboratory, Massachusetts Institute of Technology, Cambridge, Massachusetts 02139, United States

Supporting Information

ABSTRACT: Human defensin 5 (HD5) is a 32-residue host-defense peptide expressed in the gastrointestinal, reproductive, and urinary tracts that has antimicrobial activity. It exhibits six cysteine residues that are regiospecifically oxidized to form three disulfide bonds (Cys³–Cys³¹, Cys⁵–Cys²⁰, and Cys¹⁰–Cys³⁰) in the oxidized form (HD5_{ox}). To probe the solution structure and oligomerization properties of HD5_{ox} and select mutant peptides lacking one or more disulfide bonds, NMR solution studies and analytical ultracentrifugation experiments are reported in addition to *in vitro* peptide stability assays. The NMR solution structure of HD5_{ox} solved at pH 4.0 in 90:10 H₂O/D₂O, is presented (PDB: 2LXZ). Relaxation T_1/T_2 measurements and the rotational correlation time (τ_c) estimated from a ¹⁵N-TRACT experiment demonstrate that HD5_{ox} is dimeric under these experimental conditions. Exchange broadening of the H α signals in the NMR spectra suggests that residues 19–21 (Val¹⁹–Cys²⁰–Glu²¹) contribute to the dimer interface in solution. Exchange broadening is also observed for residues 7–14 comprising the loop. Sedimentation velocity and equilibrium studies conducted in buffered aqueous solution reveal that the oligomerization state of HD5_{ox} is pH-dependent. Sedimentation coefficients of ca. 1.8 S and a molecular weight of 14 363 Da were determined for HD5_{ox} at pH 7.0, supporting a tetrameric form ($[HD5_{ox}] \geq 30 \mu M$). At pH 2.0, a sedimentation coefficient of ca. 1.0 S and a molecular weight of 7079 Da, corresponding to a HD5_{ox} dimer, were obtained. Millimolar concentrations of NaCl, CaCl₂, and MgCl₂ have a negligible effect on the HD5_{ox} sedimentation coefficients in buffered aqueous solution at neutral pH. Removal of a single disulfide bond results in a loss of peptide fold and quaternary structure. These biophysical investigations highlight the dynamic and environmentally sensitive behavior of HD5_{ox} in solution, and provide important insights into HD5_{ox} structure/activity relationships and the requirements for antimicrobial action.



Host-defense peptides and proteins are key players in the mammalian innate immune response and serve to prevent colonization by invading pathogenic microbes.^{1–5} Human defensins are ribosomally synthesized, cysteine-rich, host-defense peptides expressed in neutrophils (human neutrophil peptides, HNP) and various types of epithelial cells (α - and β -defensins).^{6–9} Human defensin 5 (HD5), the focus of this work, is an α -defensin comprised of 32 amino acids that exhibits three regiospecific disulfide bonds with the connectivities Cys³–Cys³¹, Cys⁵–Cys²⁰, and Cys¹⁰–Cys³⁰ in the oxidized form, hereafter HD5_{ox} (Figure 1). Like other α -defensins, the HD5_{ox} disulfide array confers a three-stranded β -sheet structure¹⁰ and protease resistance.^{11,12}

HD5 is expressed in the human gastrointestinal,^{13–16} reproductive,¹⁷ and urinary¹⁸ tracts. Small intestinal Paneth cells,¹⁹ which reside at the base of the crypts of Lieberkühn throughout the small intestine and serve to protect the intestinal epithelium and stem cells from invading microbes, package the HD5 propeptide in subcellular granules.^{15,20} The

75-aa propeptide is converted into the 32-aa mature form by trypsin-catalyzed proteolysis of the N-terminal 43-aa pro region, and HD5 is released into the intestinal lumen in response to microbial invasion.²¹ Numerous *in vitro* studies demonstrated that HD5_{ox} exhibits antimicrobial activity against a variety of Gram-negative and -positive human pathogens including *Escherichia coli*, *Salmonella enterica*, *Bacillus cereus*, *Listeria monocytogenes*, *Staphylococcus aureus*, and *Enterococcus faecium*.^{10,22,23} A HD5 transgenic mouse, which expresses HD5 only in the small intestinal Paneth cells, survived oral *Salmonella* challenge (1.5×10^9 cfu/mL) at levels that were lethal for the wild-type mouse.²⁴ This observation supports an antibacterial role for HD5 *in vivo*. Recent HD5 transgenic mouse studies of the commensal microbiota revealed that HD5

Received: September 14, 2012

Revised: November 5, 2012

Published: November 19, 2012



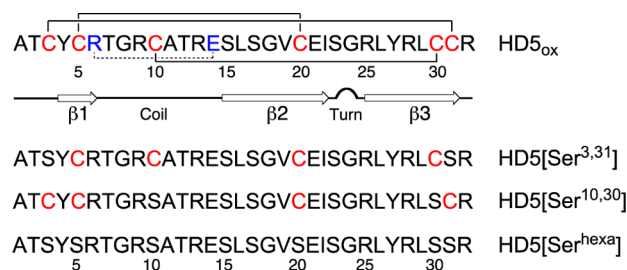


Figure 1. Primary amino acid sequences of HD5_{ox} and the mutant peptides employed in this work. The numbers refer to amino acid position. The Cys residues comprising the Cys³–Cys³¹, Cys⁵–Cys²⁰, and Cys¹⁰–Cys³⁰ disulfide linkages (solid lines) are shown in red and the residues of the Arg⁶–Glu¹⁴ salt-bridge (dashed line) are indicated in blue. The secondary structure depiction is based on the NMR solution structure presented in this work. Throughout the main text, the regiospecific disulfide linkages that define each mutant peptide are indicated in parentheses.

expression modulates the composition of the resident microflora.²⁵ Defensin deficiency has been observed in patients with inflammatory diseases of the small bowel.^{26,27} A single R13H point mutation in HD5 was observed in a Crohn's disease patient, and this mutation afforded attenuated cell killing for some bacterial species *in vitro*.²⁸ Indeed, an *E. coli* Nissle 1917 strain engineered to biosynthesize and secrete HD5 was recently reported as a possible probiotic therapy for Crohn's disease and other inflammatory diseases of the bowel.²⁹ Antiviral activities of HD5_{ox} are also documented.^{30–32} For instance, HD5_{ox} blocks infection by various nonenveloped human viruses, including adenoviruses^{31,32} and sexually transmitted papillomaviruses,³⁰ and may provide a natural barrier to certain viral diseases in the female reproductive system.

The broad-range antibacterial and antiviral activities of HD5_{ox}, in addition to other putative physiological roles, motivate investigations of structure–activity relationships. To date, these studies have addressed the importance of the arginine residues,²⁸ the role of the canonical salt bridge formed by Arg⁶–Glu¹⁴,¹¹ and the disulfide array.^{12,33} The antibacterial activity of the D-enantiomer, prepared by solid-phase peptide synthesis, was also evaluated and exhibited species-specific activity.³⁴ A recent alanine scan identified Leu²⁷ as a critical determinant for antibacterial activity.³⁵ Taken together, these investigations overwhelmingly support a model whereby the mechanism of HD5_{ox} action differs for Gram-negative (e.g., *E. coli*) and -positive (e.g., *S. aureus*) organisms. Whereas a variety of HD5 mutant peptides, including the D-enantiomer and disulfide deletion mutants, retain activity against *E. coli*, the ability of these peptides to kill *S. aureus* is severely attenuated.^{12,33,34} HD5_{ox} disrupts the Gram-negative inner membrane;¹² however, the precise details of its mechanism of action against *E. coli* and other Gram-negative organisms, in addition to how it acts on Gram-positive species, are unclear. Extensive mutagenesis studies of the human neutrophil α -defensin HNP1^{36–40} and the murine Paneth cell α -defensin cryptdin-4 (Crp4)^{41–46} have been presented. In total, these studies delineate that defensin structure/activity relationships must be considered on a case-by-case basis, and highlight the importance of evaluating both electrostatics and hydrophobicity when considering the antimicrobial and antiviral activities of human α -defensin peptides.⁴

We previously reported a HD5_{ox} mutant peptide family in which pairs of Cys residues involved in native disulfide linkages

were systematically mutated to Ser/Ala residues.¹² Many of these mutants retained antibacterial activity against *E. coli* ATCC 25922, whereas none provided activity against *S. aureus* ATCC 25923 over the concentration range tested. In addition, removal of one or more disulfide bonds markedly attenuated protease resistance. We therefore hypothesized that the lack of antibacterial activity observed for the mutant peptides against *S. aureus* may result from (i) mutant peptide instability under the assay conditions, (ii) disruption of quaternary structure, and/or (iii) failure to interact with a specific and as-yet unidentified cellular target.

Herein we address these possibilities and report extensive biophysical studies designed to probe the solution structure and dynamics of HD5_{ox} and select disulfide mutant peptides (Figure 1). We present the NMR solution structure of native HD5_{ox} in addition to NMR studies of ¹⁵N-HD5[Ser^{3,31}]_{ox}, ¹⁵N-HD5[Ser^{10,30}]_{ox}, and ¹⁵N-HD5_{red}. We also describe the quaternary structure of HD5_{ox} and disulfide mutants by using a combination of NMR dynamics measurements, rotation correlation time measurements, and analytical ultracentrifugation. These investigations demonstrate that the native disulfide array is essential for HD5_{ox} quaternary structure, and that the HD5_{ox} oligomerization state in aqueous solution is condition-dependent.

EXPERIMENTAL PROCEDURES

Materials and General Methods. All solvents, reagents, and chemicals were purchased from commercial suppliers and used as received unless noted otherwise. Deuterated water (D₂O), ¹⁵N-ammonium chloride, and U-¹³C-glucose were purchased from Cambridge Isotopes (Cambridge, MA). All aqueous solutions, buffers, and NMR samples were prepared with Milli-Q water (18.2 mΩ cm^{−1}) that was passed through a 0.22-μm filter before use. Unlabeled HD5 and mutant peptides were overexpressed as His₆-fusion proteins in *E. coli* BL21(DE3) and were purified as previously described.¹²

General Instrumentation. Analytical and semipreparative high-performance liquid chromatography (HPLC) were performed on an Agilent 1200 instrument equipped with a thermostatted autosampler set at 4 °C and thermostatted column compartment generally set at 20 °C, and a multi-wavelength detector set at 220 and 280 nm (500 nm reference wavelength unless noted otherwise). Preparative HPLC was performed using an Agilent PrepStar 218 instrument outfitted with an Agilent ProStar 325 UV–vis dual-wavelength detector set at 220 and 280 nm. A Cliepus C18 column (5 μm pore, 4.6 × 250 mm, Higgins Analytical, Inc.) set at a flow rate of 1 mL/min was employed for all analytical HPLC experiments. A ZORBAX C18 column (5 μm pore, 4.6 × 250 mm, Agilent Technologies, Inc.) set at a flow rate of 5 mL/min was employed for all semipreparative-scale HPLC purification. A Luna 100 Å C18 LC column (10 μm pore, 21.2 × 250 mm, Phenomenex) operated at 10 mL/min was utilized for all preparative-scale HPLC purification. HPLC-grade acetonitrile (MeCN) and HPLC-grade trifluoroacetic acid (TFA) were routinely purchased from EMD. For all HPLC separations, solvent A was 0.1% TFA/H₂O and solvent B was 0.1% TFA/MeCN. These solvents were passed through a 0.22-μm filter prior to use. High-resolution mass spectrometry was performed by using an Agilent LC/MS system comprised of an Agilent 1260 series LC system outfitted with an Agilent Poroshell 120 EC-C18 column (2.7 μm pore size) and an Agilent 6230 TOF system housing an Agilent Jetstream ESI source. LC/MS-grade

MeCN containing 0.1% formic acid and LC/MS-grade water containing 0.1% formic acid were obtained from J. T. Baker. For all LC/MS analyses, solvent A was 0.1% formic acid/H₂O and solvent B was 0.1% formic acid/MeCN. The samples were analyzed by using a gradient of 5–95% B over 5 min with a flow rate of 0.4 mL/min. The MS profiles were analyzed and deconvoluted by using Agilent Technologies Quantitative Analysis 2009 software version B.03.02. A BioTek Synergy HT plate reader outfitted with a calibrated BioTek Take3 Multi-Volume Plate was employed for optical absorption measurements. Peptide stock solution concentrations were routinely quantified by using the calculated extinction coefficients for HD5_{ox} or mutant peptide (Table S1, Supporting Information). Solution and buffer pH values were verified by using either a Mettler Toledo S20 SevenEasy pH meter or a HANNA Instruments HI 9124 pH meter equipped with a microelectrode.

Overexpression and Purification of ¹⁵N and ¹³C,¹⁵N-Labeled Peptides. The plasmids employed for the overexpression of His₆-Met-HD5, His₆-Met-HD5[Ser^{3,31}], and His₆-Met-HD5[Ser^{10,30}] are based on the pET-28b expression vector and are described elsewhere.¹² Each expression plasmid was transformed into homemade chemically competent *E. coli* BL21(DE3) cells and freezer stocks were prepared from single colonies. For large-scale overexpression of ¹⁵N-labeled peptides, a 50-mL overnight culture was prepared by inoculating LB media containing 50 µg/mL kanamycin from a freezer-stock of the desired *E. coli* overexpression strain. The starter culture was grown for 16 h (37 °C, 175 rpm) and the OD₆₀₀ was recorded to confirm that the cultures reached saturation (OD₆₀₀ ~ 1.5). Aliquots (20 mL) of the overnight culture were centrifuged (3600 rpm × 10 min, 4 °C) and the supernatant was discarded. Each resulting cell pellet was resuspended in 3 mL of sterile-filtered ¹⁵N-labeled M9 minimal medium (6.0 g/L disodium phosphate, 3.0 g/L monopotassium phosphate, 0.5 g/L sodium chloride, 1.0 g/L ¹⁵N-labeled ammonium chloride) supplemented with 2 mL/L of 1 M MgSO₄, 2 mL/L of 5 mM FeCl₃, 100 µL/L of 1 M CaCl₂, 1 mL/L of glycerol, 2.0 g/L of D-glucose, 1 mL/L of 50 mg/mL kanamycin, and 200 µL of a vitamin mix.⁴⁷ The vitamin mix contained choline chloride (200 mg), folic acid (250 mg), pantothenic acid (250 mg), nicotinamide (250 mg), myo-inositol (50 mg), pyridoxal hydrochloride (250 mg), thiamin hydrochloride (250 mg), riboflavin (25 mg), adenosine (50 mg), and biotin (50 mg) suspended in 7.5 mL of sterile-filtered Milli-Q water. Each resuspended bacterial cell pellet was used to inoculate 1 L of the same minimal medium, and the resulting cultures were grown at 37 °C with shaking at 175 rpm in 4 L baffled flasks. Protein expression was induced by addition of IPTG (0.5 mL of a 0.5 M aqueous stock solution, 250 µM final concentration) at OD₆₀₀ ~ 0.6 (*t* ~ 5.5 h). The cultures were incubated at 37 °C with shaking at 175 rpm for an additional 5.5 h, and the cells were immediately pelleted by centrifugation (4000 rpm × 30 min, 4 °C). ¹⁵N-Labeled HD5_{ox} was overexpressed on a 4-L scale and the ¹⁵N-labeled mutant peptides were each overexpressed on a 12-L scale. The final OD₆₀₀ values varied from ca. 0.7 to ca. 1.2 depending on the shaker flask. The resulting cell pellets were collected, flash frozen in liquid N₂, and stored at –80 °C. The wet pellet yield for ¹⁵N-His₆-Met-HD5 was ca. 2 g/L culture. Wet pellet yields of ca. 1.2 and ca. 1.8 g/L culture were obtained for ¹⁵N-His₆-Met-HD5[Ser^{3,31}] and ¹⁵N-His₆-HD5[Ser^{10,30}], respectively. Overexpression of double-labeled ¹³C,¹⁵N-His₆-Met-HD5 was performed on a 6-L scale by using

the same method and substituting U-¹³C-glucose for unlabeled glucose.

Isotopically-labeled His₆-HD5 and the His-tagged mutant peptides were purified as described previously for the unlabeled congeners.¹² In brief, the His₆-tagged HD5 and serine double mutants were isolated in yields of ca. 5–15 mg/L culture following Ni-NTA affinity chromatography. Each His₆ tag was cleaved by using cyanogen bromide, and each crude peptide was reduced by addition of TCEP and HPLC purified. An oxidative folding procedure was employed to obtain the oxidized forms, which were separated and purified by semipreparative HPLC.¹² Peptide purity was ascertained by analytical HPLC (Figures S1–S4), and peptide identities were confirmed by mass spectrometry (Table S2). The purified peptides were lyophilized to dryness and stored as powders at –20 °C until use. Some disulfide bond shuffling was observed by analytical HPLC for several unlabeled disulfide deletion mutants after several months of storage at –20 °C in neutral aqueous solution. As a result, the ¹⁵N-labeled disulfide regioisomers of the serine double mutants were stored as lyophilized powders until use.

Peptide Stability in the Presence of *Staphylococcus aureus*. *S. aureus* ATCC 25923 was grown overnight with shaking (37 °C, 16 h) in 5 mL of TSB. The overnight culture was diluted 1:100 into 6 mL of fresh TSB and grown for ~2 h at 37 °C with shaking at 150 rpm until the OD₆₅₀ reached ~0.6. A 5-mL portion of the culture was transferred to a sterile culture tube and centrifuged (3500 rpm × 10 min, 4 °C) to pellet the bacterial cells. The supernatant was discarded and the cell pellet was resuspended in 5 mL of AMA buffer (10 mM sodium phosphate buffer supplemented with 1% TSB, pH 7.4). The cell suspension was centrifuged (3500 rpm × 10 min, 4 °C) and the supernatant was discarded. The resulting cell pellet was resuspended in 5 mL of AMA buffer and diluted with AMA buffer to obtain an OD₆₅₀ value of 0.6 (1 × 10⁸ CFU/mL). This bacterial suspension was further diluted 1:100 in two steps (1:10 × 1:10) into 2 mL of AMA buffer. The diluted cultures were used immediately.

Peptide stability assays were performed in 96-well plates. Each well contained 10 µL of a 200-µM (10×) aqueous sterile-filtered peptide stock solution or a no-peptide control. A 90-µL aliquot of the diluted bacterial culture was added to each well and the plate was incubated for 1 h (37 °C, 150 rpm). Wells containing AMA buffer only and peptide in the AMA buffer without *S. aureus* were also included. Immediately after the 1-h incubation, each culture was transferred to a microcentrifuge tube and the samples were centrifuged (13 000 rpm × 10 min, 4 °C). The supernatants were transferred to new microcentrifuge tubes, a 10-µL aliquot of 2% aqueous TFA was added to each solution, and the samples were centrifuged (13 000 rpm × 10 min, 4 °C). The resulting supernatants were transferred to HPLC vials and stored in an autosampler thermostatted at 4 °C until analytical HPLC analysis (10–60% B over 30 min). This assay was conducted at least in triplicate for each peptide and over two separate days. Representative HPLC traces are reported in Figures 2 and S5–S6.

Solution NMR Sample Preparation. Samples of ¹⁵N-HD5_{ox} were prepared at different concentrations and pH values to determine the optimal sample conditions for NMR data collection. Initial data acquisition was performed on a 460-µM sample of ¹⁵N-HD5_{ox} that was dissolved in 90:10 H₂O/D₂O immediately after HPLC purification and lyophilization (Figure 3). Additional samples of ¹⁵N-HD5_{ox} were prepared at pH 5.0

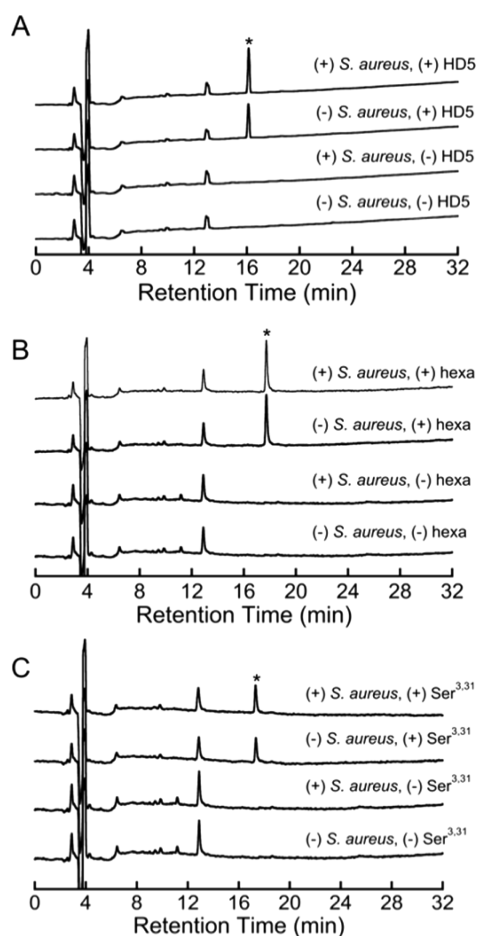


Figure 2. Analytical HPLC traces of *S. aureus* culture supernatants (10 mM sodium phosphate buffer supplemented with 1% TSB, pH 7.4) treated with 20 μ M of HD5_{ox} or a mutant peptide for 1 h at 37 °C. (A) HD5_{ox}. (B) HD5[Ser^{hexa}]. (C) HD5[Ser^{3,31}] (5–10)(20–30). Absorption at 220 nm was monitored with a reference wavelength of 500 (A) or 360 nm (B and C) (10–60% B in 30 min). In each panel, the star indicates the peak corresponding to the defensin peptide. Traces for other HD5 mutants are provided as Supporting Information.

(630, 460, and 260 μ M) by using an aqueous solution of 1 N HCl for adjusting the sample pH. In a separate screen, ^{15}N -HD5_{ox} samples at pH 7.0 (333 μ M), 6.0 (340 μ M), 5.0 (400 μ M), and 4.0 (460 μ M) in 90:10 H₂O/D₂O were prepared by using TFA to adjust pH as necessary. To determine the effect of buffer, samples of ^{15}N -HD5_{ox} (800 μ M) were prepared in 20 mM Tris-HCl buffer containing 10% D₂O (v/v) at pH = 7.0, 6.0, and 5.0. Lastly, ^{15}N -HD5_{ox} (880 μ M) was prepared in 10 mM sodium phosphate buffer with 10% D₂O (v/v) at pH = 7.0, 6.0, and 4.0. In these two sets of samples, the sample pH was adjusted by incremental additions of 1 N HCl. On the basis of the ^1H , ^{15}N -HSQC spectra of ^{15}N -HD5_{ox} prepared under various conditions, the ^{13}C , ^{15}N -HD5_{ox} sample (340 μ M) was prepared in 90:10 H₂O/D₂O at pH 4.0, and TFA was employed to adjust the sample pH. These conditions afforded the greatest peak dispersion, and 28 of 31 amide resonances were observed for ^{13}C , ^{15}N -HD5_{ox} in the ^1H , ^{15}N -HSQC spectrum. Likewise, all ^{15}N -HD5[Ser^{3,31}]_{ox} and ^{15}N -HD5-[Ser^{10,30}]_{ox} regioisomers were prepared in 90:10 H₂O/D₂O at pH 4.0. The NMR sample of ^{15}N -HD5_{red} (650 μ M) was

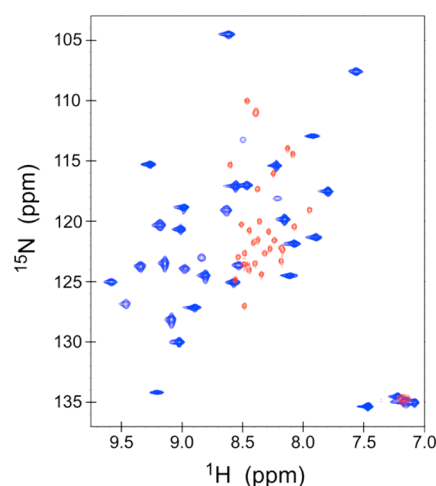


Figure 3. Overlay of ^{15}N -HD5_{ox} (blue) and ^{15}N -HD5_{red} (red) ^1H , ^{15}N -HSQC spectra recorded on a 600 MHz spectrometer. The concentration of HD5_{red} was 650 μ M, and the sample was prepared in 90:10 H₂O/D₂O containing 20 μ M TFA. The HD5_{ox} sample concentration was 460 μ M, and the sample was prepared in 90:10 H₂O/D₂O immediately after HPLC purification and lyophilization, and no pH adjustment was performed.

prepared in 90:10 H₂O/D₂O containing 20 μ M TFA to ensure that the peptide remained reduced.

Solution NMR Spectroscopic Studies. All 1-D ^1H NMR spectra were collected on a Varian 500 MHz spectrometer housed in the MIT Department of Chemistry Instrumentation Facility (DCIF) that was operated at an ambient probe temperature of 293 K (Figures S7 and S8). Standard techniques for water suppression and data acquisition were employed. A number of multidimensional NMR spectra were recorded on a 600 MHz NMR spectrometer housed in the MIT Francis Bitter Magnet Laboratory (FBML) based on a FBML narrow bore magnet and a console designed and constructed by members of the FBML. This spectrometer is equipped with three transmitter channels, and a Nalorac 5 mm indirect triple resonance ^1H [^{13}C , ^{15}N] probe with z-gradient. Additional multidimensional NMR spectra were recorded on a 600 MHz Bruker Avance spectrometer equipped with a cryogenic probe housed at Harvard Medical School. To determine optimal acquisition conditions for HD5_{ox} ^1H , ^{15}N -HSQC experiments were performed at 15, 20, and 25 °C. For the initial resonance assignments, TOCSY and NOESY experiments were performed at 25 °C. 2-D TOCSY spectra were recorded with mixing times of 30 and 60 ms, and 2-D NOESY spectra were recorded with mixing times of 150, 200, and 400 ms. All experiments were acquired with 2048 complex points in t_2 and 512 complex points in t_1 , and a sweep width of 12 ppm in both dimensions. The 3-D ^{15}N -edited TOCSY and 3-D ^{15}N -edited NOESY experiments were collected with 60 and 200 ms mixing times, respectively. A 200 ms mixing time was also employed for a 3-D ^{13}C -edited NOESY experiment. Sequence-specific assignment was aided by the collection of standard HNCA, HNCO, and HNCACO pulse sequences; however, nonuniform sampling was used. Specifically, a matrix of 38 points (^{15}N dimension) by 40 points (^{13}C dimension) at the ca. 20% level (a total of 320 acquired complex points) was subsampled. The sampling schedule was created based on the Poisson Gap sampling method.⁴⁸ Missing data points were reconstructed by using the istHMS algorithm.⁴⁹ Only 1-D ^1H NMR and 2-D

^1H , ^{15}N -HSQC spectra for the HD5[Ser^{3,31}]_{ox} and HD5-[Ser^{10,30}]_{ox} regioisomers were collected, and the HSQC experiments were conducted over a temperature range of 15–25 °C. Spectral data were processed by using NMRPipe⁵⁰ and analyzed by using Sparky⁵¹ or CARA.⁵²

NMR Solution Structure Calculations and Refinement.

Structure calculations were initially performed in CYANA to fully assign NOE crosspeaks and establish the hydrogen bond network by inference from preliminary structures along with NOE patterns. These NOE assignments were then used in structure calculations with X-PLOR NIH using explicit water refinement. During this calculation, the system was cooled from 3000 to 25 K within 10 ps, applying the high force constants obtained at the end of the previous cooling stage. The experimental restraints included 421 upper distance limits, 54 dihedral angles identified by analysis of backbone chemical shifts by the program TALOS,⁵³ 16 χ_1 angles, 3 disulfide bonds, and 15 hydrogen bonds.

Of the 400 structures resulting from the final round of structure calculation, the 20 lowest-energy structures were selected. The geometry and elements of secondary structure were analyzed using PROCHECK.⁵⁴ These coordinates are deposited in the Protein Data Bank (code: 2LXZ). The UCSF Chimera⁵⁵ package and MOLMOL⁵⁶ were employed for final graphical presentation.

Sedimentation Velocity Experiments. A Beckman XL-I Analytical ultracentrifuge outfitted with an An-50 Ti rotor was employed for all sedimentation velocity (SV) experiments. The rotor housed conventional double-sector charcoal-filled Epon centerpieces within the sample cells and contained either sapphire (Rayleigh interference optics) or quartz (absorption optics) windows. The absorption wavelength for optical detection was 280 nm, and the interferometer laser wavelength was 660 nm. The samples were centrifuged at 42 000 rpm and 20 °C until sedimentation was complete. SEDNTERP⁵⁷ was employed to calculate the buffer viscosity (η), buffer density (ρ), and protein partial specific volume (\bar{v}) values at 20 °C based on a database of known values available via the Internet (<http://www.jphilo.mailway.com>). The sedimentation coefficients were subsequently calculated by fitting the sedimentation velocity data using SEDFIT. The continuous distribution $c(s)$ Lamm equation model, which accounts for protein diffusion, was employed.⁵⁸ The sedimentation coefficients generated by this approach were confirmed by using DCDT+.^{59,60} The apparent sedimentation coefficient distribution, $g(s^*)$, was generated from 22 to 26 scans with a peak broadening limit of 60 kDa using DCDT+.

All SV window assemblies were loaded with 410 μL of buffer reference and 400 μL of peptide sample, and the buffers and samples were prepared immediately before the SV runs. In one set of experiments, samples of HD5_{ox}, the HD5[Ser^{3,31}]_{ox} and HD5[Ser^{10,30}]_{ox} regioisomers, and HD5[Ser^{hexa}] were prepared at pH 7.0 in 10 mM sodium phosphate buffer. A solution of 1 N HCl was employed to adjust pH. Starting from a lyophilized peptide sample, a concentrated stock solution of each peptide was prepared from buffer that was filtered through a 0.45- μm membrane. In microcentrifuge tubes, aliquots of the peptide stock solution were diluted to 400 μL with buffer to provide the desired concentrations and subsequently transferred to the AUC sample cells. Samples at the following peptide concentrations were prepared and analyzed: HD5_{ox}, 30, 50, 80, 115, 120, 183, 186, 283, 301, 303, 424, and 437 μM ; HD5[Ser^{3,31}]_{ox} (5–20)(10–30), 60, 62, 65, 90, and 131 μM ;

HD5[Ser^{3,31}]_{ox} (5–30)(10–20), 105, 136, and 201 μM ; HD5[Ser^{3,31}]_{ox} (5–10)(20–30), 74, 105, 153, and 210 μM ; HD5[Ser^{10,30}]_{ox} (3–20)(5–31), 153, 180, 224, and 236 μM ; HD5[Ser^{10,30}]_{ox} (3–31)(5–20), 57, 232, and 396 μM ; HD5[Ser^{hexa}], 90 and 91 μM .

Additional SV experiments were conducted to evaluate the consequences of pH, salt, and buffer components on the sedimentation of HD5_{ox}. In all cases, the 400- μL solutions were prepared as described above and the buffer pH was adjusted by using 1 N HCl. To determine the effect of pH, samples of HD5_{ox} in 10 mM sodium phosphate buffer were adjusted to pH values of 6.0 (161 μM), 4.0 (131 μM), and 2.0 (194 μM). To ascertain the effect of NaCl, samples of HD5_{ox} at pH 7.0 in 10 mM sodium phosphate buffer containing 50 mM (183, 283 μM), 150 mM (181, 278 μM), and 500 mM (178, 270 μM) NaCl were prepared. To evaluate the effects of buffer choice and divalent cations, sedimentation of HD5_{ox} was investigated at pH 7.0 in 20 mM Tris-HCl or 20 mM HEPES buffer with or without 50 mM MgCl₂ or CaCl₂. For the experiments in Tris buffer, the HD5_{ox} concentrations were 126 and 210 μM (no divalent cations), 170 and 236 μM (+Mg), or 128 and 157 μM (+Ca). For the experiments in HEPES buffer, the HD5_{ox} concentrations were 191 and 256 μM (no divalent cations), 131 and 190 μM (+Mg), and 191 and 212 μM (+Ca).

Hydrodynamic modeling computations were performed with HYDROPRO⁶¹ to calculate sedimentation coefficients for the HD5_{ox} monomer, dimer, and tetramer (Table S3). Both the HD5_{ox} monomer NMR solution structure presented in this work and the reported HD5_{ox} crystal structure (PDB: 1ZMP)¹⁰ were employed in hydrodynamic modeling. All HYDROPRO calculations used the buffer density (ρ) and buffer viscosity (η) values for water at 20 °C, and a partial specific volume (\bar{v}) of 0.7094 mL/g for HD5_{ox}. Equation 1 was employed to calculate sedimentation coefficients for HD5_{ox} modeled as a smooth, compact, and spherical peptide in water at 20 °C using the classical combination of the Svedberg and Stokes equation.⁵⁸ The values are reported in Table S4. Equation 1 states

$$s_{\text{sphere}} = 0.012 \frac{M^{2/3}(1 - \bar{v}\rho)}{\bar{v}^{1/3}} \quad (1)$$

where s_{sphere} is the sedimentation coefficient for an ideally sedimenting sphere in S units, M is the molar mass of the macromolecule in Daltons, \bar{v} is in milliliters per gram, and ρ is in grams per milliliter. To ascertain the maximum shape asymmetry from a sphere, the minimum frictional ratios were calculated with Equation 2

$$s_{\text{sphere}}/s_{20,w} = f/f_0 \quad (2)$$

where $s_{20,w}$ is the sedimentation coefficient for the peptide in water at 20 °C, f is the experimental frictional coefficient, and f_0 is the minimal frictional coefficient. The maximum shape asymmetry was determined for HD5_{ox} in different buffers, HD5[Ser^{hexa}], HD5[Ser^{3,31}]_{ox} and HD5[Ser^{10,30}]_{ox}. Each f/f_0 analysis for the disulfide deletion mutants was performed by using the average $s_{20,w}$ value determined from all regioisomeric disulfide pairings (Table S5).

Sedimentation Equilibrium Experiments. The Beckman XL-I Analytical ultracentrifuge outfitted with an An-50 Ti rotor described above was employed for all sedimentation equilibrium (SE) experiments. The absorption wavelength for optical detection was 280 nm, and the instrument was maintained at 20 °C. Samples (400 μL) of HD5_{ox} were prepared in 10 mM

sodium phosphate buffer at pH 8.0 (183, 230, and 283 μM), 7.0 (165, 187, 225, 238, 283, and 288 μM), 6.0 (210 and 330 μM), 4.0 (236, and 288 μM), and 2.0 (189, 238, and 293 μM) as described above. Equilibrium profiles were established at rotor speeds of 20 000, 25 000, and 36 000 rpm based on sedimentation coefficients of ~ 1.8 S obtained from the SV experiments.⁶² Upon equilibrium establishment, 10 scans with 5 replicates were recorded.

SEDNTERP⁵⁷ was employed to calculate the buffer viscosity (η), buffer density (ρ), and protein partial specific volume (\bar{v}) values at 20 °C as described above. Molecular weights were determined by global fitting of the multispeed equilibrium data across at all loading concentrations at a given pH value using the program SEDPHAT.⁶³ The Species Analysis model and Single Species of an Interacting System model, both with mass conservation, were employed for data analysis with the bottom of the sample sector assigned as a floating parameter. To further verify whether each least-squares curve-fitting procedure converged to a global minimum, the alternate methods of Simplex, Marquardt–Levenberg, and simulated annealing were employed to assess any change in the global reduced chi-squared value.

RESULTS

Peptide Stability in the Presence of *S. aureus*. Figure 2 presents the analytical HPLC traces obtained for supernatants of *S. aureus* cultures treated with HD5_{ox}, HD5[Ser^{3,31}] (5–10)(20–30), and HD5[Ser^{hexa}]. Traces for additional mutants are provided as Supporting Information (Figures S5 and S6). In all cases, the peak corresponding to the peptide of interest exhibited comparable intensity whether or not *S. aureus* was included in the well. No new peaks in the analytical HPLC traces attributable to peptide degradation formed. These observations demonstrate that HD5_{ox} and the disulfide mutant peptides are stable under the conditions previously employed for assaying antibacterial activity against *S. aureus*.¹² The attenuated activity of the mutant peptides reported previously results from neither peptide degradation nor disulfide bond reshuffling to an inactive form during the course of the assay.¹²

Overexpression and Purification of Isotopically-labeled Peptides. ¹⁵N- and ¹³C,¹⁵N-labeled HD5_{ox} were obtained in yields of ca. 100 $\mu\text{g/L}$ culture following overexpression of His₆ fusion proteins in M9 minimal media containing a vitamin supplement, Ni-NTA purification, His₆ tag cleavage, purification of the reduced form, and oxidative folding. This procedure was extended to the HD5[Ser^{3,31}]_{ox} and HD5[Ser^{10,30}]_{ox} peptides, which were obtained in yields of ca. 100 and ca. 300 $\mu\text{g/L}$, respectively. All isotopically labeled peptides were obtained in high purity (Figures S1–S4), and the identities were confirmed by mass spectrometry (Table S2). Although adequate for NMR studies, these yields are lower than the yields reported for peptide overexpression in nutrient-rich medium.¹² This decreased yield is largely attributed to variability in culture growth, ascertained by OD₆₀₀ values, in minimal media. In several instances, the OD₆₀₀ value remained ≤ 0.7 following induction and continued incubation at 37 °C. This phenomenon was unpredictable, and we therefore collected the cell pellets ca. 5.5 h after induction and independent of OD₆₀₀ value at that time point. The HD5[Ser^{5,20}] peptides were not considered in this work because low yields of the unlabeled His-tagged peptides were achieved previously in nutrient-rich medium.¹²

NMR Solution Structure Determination of HD5_{ox}. A preliminary ¹H,¹⁵N-HSQC spectrum of ¹⁵N-HD5_{ox} in 90:10 H₂O/D₂O revealed 31 well-resolved amide resonances, which supported the presence of one folded species in solution (Figure 3). In contrast, markedly decreased peak dispersion was observed for ¹⁵N-HD5_{red} in 90:10 H₂O/D₂O containing 20 μM TFA (Figure 3), indicating that HD5_{red} is unfolded. The loss of fold upon peptide reduction is in agreement with prior circular dichroism studies of HD5,¹² and a qualitative comparison of the ¹H,¹⁵N-HSQC spectra of oxidized and reduced human β -defensin 1.⁶⁴ Screenings of sample conditions and acquisition parameters to delineate the optimal conditions for data collection and solution structure determination were subsequently conducted. The ¹H,¹⁵N-HSQC spectra obtained for ¹⁵N-HD5_{ox} prepared in Tris or sodium phosphate buffer over the pH range of 5–7 were markedly different than the spectra of the unbuffered sample presented in Figure 3. Specifically, peaks were broader, less dispersed, and more heterogeneous in intensity for the buffered samples (Figures S9 and S10). Differences in the ¹H,¹⁵N-HSQC spectra were also observed for unbuffered ¹⁵N-HD5_{ox} prepared in 90:10 H₂O/D₂O that was pH adjusted with HCl or TFA (Figures S11–S13). Variations in acquisition temperature and sample concentration had negligible impact on chemical shift dispersion over the evaluated ranges (Figure S12). These exploratory studies highlighted the importance of sample preparation on dynamic exchange events, and further spectroscopic experiments were conducted in 90:10 H₂O/D₂O with the sample pH adjusted to 4.0 by TFA addition.

2-D homonuclear NOESY and TOCSY spectra were employed for initial ¹⁵N-HD5_{ox} sequence-specific assignments, using the established methods of Wüthrich.⁶⁵ These spectra were insufficient to complete sequence-specific assignment because of significant attenuation of many backbone amide signals and poor NOE data, which were most likely the results of exchange broadening. Only ca. 50% of the molecule could be assigned by using this approach, and with low confidence. A sample of ¹³C,¹⁵N-HD5_{ox} was therefore prepared, and standard triple-resonance spectra (HNCO, HNCA, HNCACO) were collected to aid in backbone assignment. In addition, 3-D ¹³C-edited and 3-D ¹⁵N-edited NOESY spectra of ¹³C,¹⁵N-HD5_{ox} were recorded. These spectra, together with the homonuclear experiments, permitted almost complete sequence-specific assignment of the HD5_{ox} backbone (87.5% of the backbone assigned) and an overall assignment of 89.7% for the entire molecule (Figure S14). This assignment was sufficient for structure determination. Further assignment was hampered by exchange broadening of signals (Figure S15, *vide infra*). Additionally, backbone chemical shift assignment of the heavy nuclei provided information on backbone dihedral angles. Preliminary CYANA structure calculations confirmed beta-sheet elements, and the H-bonding network was established by the proximity of interresidue NOEs. Previous crystallographic studies of synthetic HD5_{ox} revealed the α -defensin disulfide bonding pattern of Cys³–Cys³¹, Cys⁵–Cys²⁰, and Cys¹⁰–Cys³⁰.¹⁰ In this work, characteristic intercysteine NOEs were observed between these pairs of cysteine residues (Table S6, Figure S16). Moreover, initial structure calculations were consistent with this arrangement of the disulfide bonds without explicitly declaring them in the calculation. Covalent disulfide bonding restraints for Cys³–Cys³¹, Cys⁵–Cys²⁰, and Cys¹⁰–Cys³⁰ were therefore included in the final structure calculations (Figure S17). The final collection of 20 lowest-energy

Table 1. Structure Statistics for the Solution Structure of HD5_{ox}

	<SA>	(SA) _r
r.m.s. deviations from NOE restraints (Å) ^a		
all (421)	0.032 ± 0.003	0.056
sequential [i - j = 1] (151)	0.035 ± 0.004	0.052
medium range [i - j ≤ 4] (53)	0.027 ± 0.005	0.074
long-range [i - j ≥ 5] (133)	0.024 ± 0.006	0.066
intraresidue (84)	0.035 ± 0.008	0.045
r.m.s. deviations from dihedral angles restraints (°) ^b	0.044 ± 0.017	0.877
Deviation from idealized covalent geometry		
bonds (Å)	0.011 ± 0.006	0.004
angles (°)	0.573 ± 0.081	0.523
impropers (°)	0.250 ± 0.073	0.493
Ramachandran results (%) ^c		
most favorable region	85.6 ± 3.8	92.6
additionally allowed region	14.4 ± 3.8	7.4
generously allowed region	0.0 ± 0.0	0.0
disallowed region	0.0 ± 0.0	0.0
Coordinate precision (Å) ^{d,e}		
protein backbone	0.135 ± 0.034	
protein heavy atoms	0.806 ± 0.102	

^aNone of the structures exhibited distance violations greater than 0.5 Å or dihedral angle violations greater than 5°. ^bThe experimental dihedral angle restraints were as follows: 26 ϕ , 25 ψ , and 15 χ_1 angular restraints. ^cDetermined using the program PROCHECK.⁵⁴ ^dThe coordinate precision is defined as the average atomic root-mean-square deviation (RMSD) of the 20 individual SA structures and their mean coordinates. Backbone atoms are N, C α , and C'. ^eStructure calculations also included 15 hydrogen bonds. These bonds were included in X-PLOR structure calculations as HBDB terms as described in ref 81.

structures was generated with explicit water refinement, which provided a backbone RMSD of 0.135 Å for the heavy atom backbone over the full length of the peptide (Table 1). The solution structure was determined for the HD5_{ox} monomer because intermolecular NOEs were not reliably observed. The lack of intermolecular NOEs most likely results from exchange broadening of the H α signals at the dimer interface (*vide infra*).

The overall fold of HD5_{ox} exhibits a three-stranded beta-sheet characteristic of α -defensins (Figure 4). Strand β 1 consists of residues 4–6, β 2 is comprised of residues 15–22, and β 3 extends from residues 25–31. Strands β 2 and β 3 are connected by a tight beta type-I turn defined by Ser²³-Gly²⁴ (Figures 1 and 4). The three beta-sheets constitute 65% of the tertiary structure (Figure S18). This beta-sheet content is greater than that observed for Crp4 (34%)⁴³ and similar to the beta-sheet content (60%) of HNP3.⁶⁶ Residues 7–14 form a loop of irregularly structured secondary structure. The presence of the Arg⁶-Glu¹⁴ salt bridge is apparent from observed NOE interactions with neighboring residues. The five additional Arg residues are positioned on one face of the structure, and on the opposite side of the predominantly hydrophobic Ser¹⁵-Ile²² β -sheet (Figures 4C and S19). This clustering of hydrophobic and hydrophilic residues provides amphipathic character.

NMR Solution Studies of HD5_{ox} Quaternary Structure and Dynamics. Evaluation of the oligomerization state of the ¹³C,¹⁵N-HD5_{ox} NMR sample was evaluated through T_1/T_2 data, a ¹⁵N-TRACT experiment, and calculations of rotational correlation time (τ_c). T_1 values were measured using the standard inversion-recovery method, and T_2 data were obtained

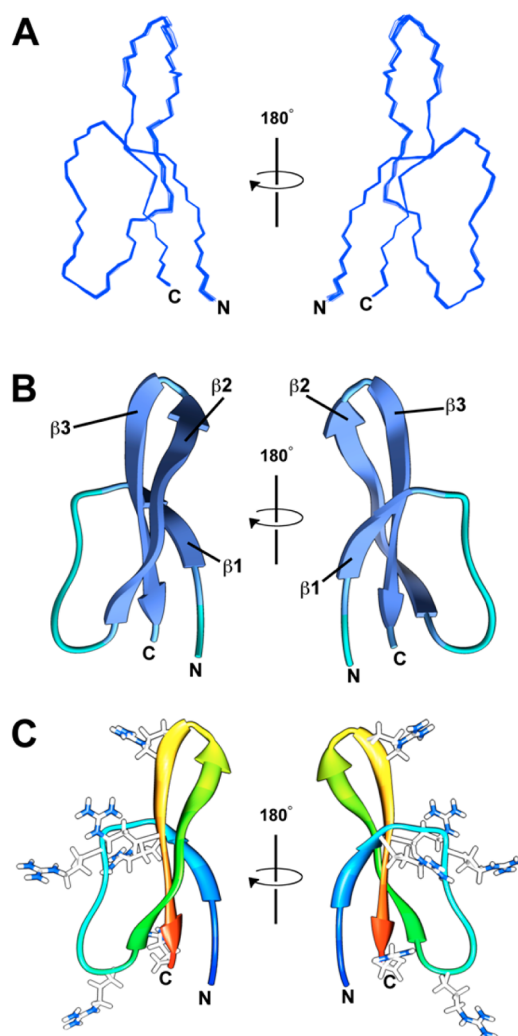


Figure 4. NMR solution structure of 340 μ M ¹³C,¹⁵N-HD5_{ox} in 90:10 H₂O/D₂O at pH 4.0. (A) Overlay of the best 20 structures selected from 400 calculated conformers. RMSD for backbone atoms, 0.135 Å; RMSD for heavy atoms, 1.352 Å. (B) Ribbon diagrams illustrating the β -sheet structure of HD5_{ox}. (C) Depiction of the arrangement of the six Arg residues.

from a Carr-Purcell-Meiboom-Gill (CPMG) relaxation dispersion experiment. T_1/T_2 data for the well-structured beta-turn region were used to estimate correlation times. The average T_2 value from this beta-turn region defined by Ile²²-Leu²⁶ is 181.2 ms, which corresponds to a τ_c of ca. 3.5–3.7 ns. The τ_c was also determined using the ¹⁵N-TRACT method, which relies on the transverse relaxation optimized spectroscopy (TROSY) principle.⁶⁷ This method gives estimates of τ_c that are independent of exchange phenomenon, which can complicate the interpretation of T_2 measurements. This approach afforded a τ_c value of ca. 4.1 ns, which is in good agreement with the T_2 analysis of the beta-turn loop and estimates a molecular weight of ca. 6.8 kDa. Both methods indicate that HD5_{ox} exists as a dimer under the NMR sample conditions.

Outside of the Ile²²-Leu²⁶ beta-turn region, the T_2 values are highly variable, whereas the T_1 values are nearly equal (Figure 5A). Many residues exhibit T_2 values that are shorter than the T_2 values for the Ile²²-Leu²⁶ beta-turn region (e.g., residues 5–7, 10–14, 16–17, 19, 27, 30, 31), indicating that these residues

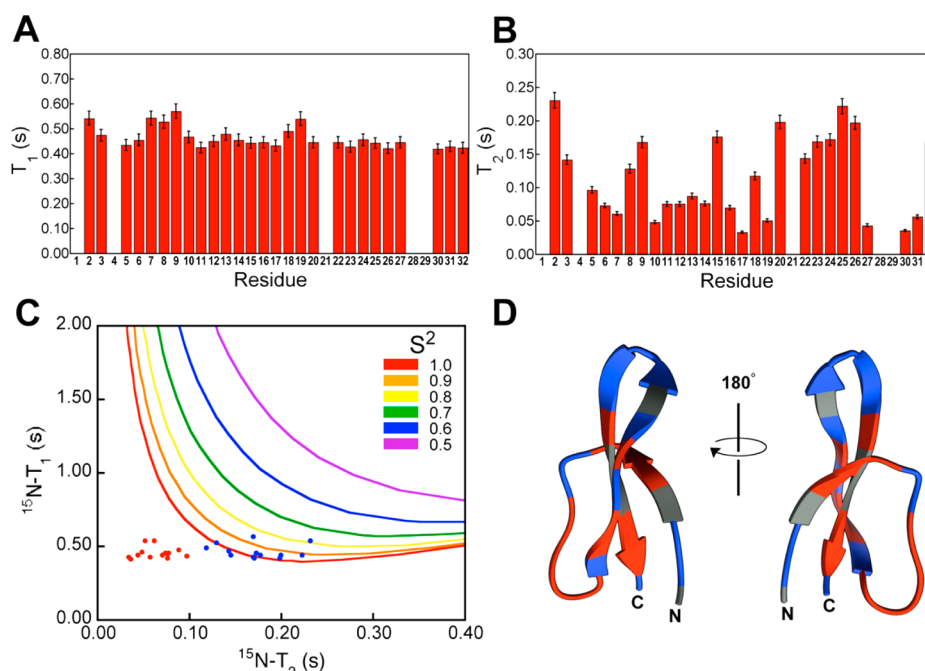


Figure 5. Relaxation studies and dynamics of 340 μM ^{13}C , ^{15}N -HD5_{ox} in 90:10 H₂O/D₂O at pH 4.0. (A) T_1 data. (B) T_2 data. (C) Plot of T_1 versus T_2 with theoretical order parameters (S^2 values) for data collected at 600 MHz. Red dots: Residues with $T_2 < 0.12$ s. Blue dots: Residues with $T_2 > 0.12$ s. (D) NMR structure of HD5_{ox} where T_2 values < 0.12 s or > 0.12 s are colored in red or blue, respectively. The gray regions indicate unobserved residues.

may undergo conformational exchange broadening (Figure 5B). To determine whether these residues are indeed exchange broadened, we plotted T_1 values versus T_2 values (Figure 5C). In addition, we overlaid the theoretical values of T_2 and T_1 for a range of correlation times using the standard ‘Model Free’ formalism of Lipari and Szabo^{68,69} and for various order parameters (S^2 values) for data collection at 600 MHz. A S^2 value of 1.0 indicates a rigid structure, whereas lower S^2 values point to flexibility on the microsecond or faster time scale. Figure 5C reveals that many residues fall to the left of the $S^2 = 1.0$ line, indicating that these residues are most likely exchange broadened on a time scale of milliseconds. This large amount of exchange broadening is consistent with the difficulties encountered in assigning the backbone of HD5_{ox}.

NMR Solution Studies of Disulfide Deletion Mutants. 1-D ^1H and 2-D ^1H , ^{15}N -HSQC NMR spectra were recorded for all regioisomers of HD5[Ser^{3,31}]_{ox} and HD5[Ser^{10,30}]_{ox} (Figures S7, S8, and S20–S26). In all cases, the chemical shift dispersion of the amide HN region was less than 1 ppm and comparable to the dispersion observed for unstructured HD5_{red} (Figure 3). Moreover, many of these spectra exhibited greater than 31 amide resonances, which suggested that multiple species exist in aqueous solution at pH 4.0. The disulfide deletion mutant peptides each lack structural organization in aqueous solution. As a result, no further NMR spectroscopic characterization of these peptides was pursued.

Sedimentation Velocity Studies of HD5_{ox} Quaternary Structure. A series of SV experiments was conducted to evaluate the sedimentation behavior of HD5_{ox} under a variety of conditions, and the results from all SV experiments are summarized as Supporting Information (Tables S7–S11 and Figures S27–S30). At pH 7.0 in 10 mM sodium phosphate buffer, conditions similar to those routinely employed for *in vitro* defensin antibacterial activity assays,¹² a single peak at 1.8

S is observed over the range $s_{20,w} = 0.7\text{--}3.7$ S in both the Gaussian fit of the observed $g(s^*)$ peak and in $c(s)$ (Figure 6). The Gaussian fit supports the existence of a single species, and the single peak in $c(s)$ precludes the presence of fast association kinetics between various oligomeric states.⁶⁰ To evaluate whether the S-value exhibits concentration dependence, HD5_{ox} samples ranging from 30 to 437 μM were evaluated (Figure S27). In all cases, one sedimentation coefficient of ca. 1.8 S was obtained by the $g(s^*)$, $c(s)$, and dc/dt methods (Table S7), which supports a monodisperse oligomerization state at pH 7.0 over this concentration range and also suggests a dissociation constant below 30 μM for the 1.8 S species.

The HD5_{ox} S-value decreased as the pH was lowered from 7.0 to 2.0 across a range of sample concentrations (10 mM sodium phosphate buffer). Sedimentation coefficients of 1.8 S (pH 7.0), 1.6 S (pH 6.0), 1.2 S (pH 4.0), and 1.0 S (pH 2.0) were obtained by DCDT+ analysis, which provided evenly distributed single-Gaussian fitting of the absorbance raw data as corrected $s_{20,w}$ values (Table S8, Figure S28).

Substitution of phosphate buffer with Tris or HEPES buffer had a negligible effect on the sedimentation of HD5_{ox} at pH 7.0 (Tables S9 and S10 and Figure S29). Average sedimentation coefficients of ca. 1.6 S over a range of peptide concentrations were obtained for HD5_{ox} in Tris or HEPES buffer, respectively. Moreover, millimolar concentrations of Mg(II) and Ca(II) had negligible impact on the HD5_{ox} sedimentation coefficient when added to either Tris or HEPES buffer at pH 7.0 (Tables S9 and S10 and Figure S29). These data demonstrate that physiological concentrations of Mg(II) and Ca(II) do not influence HD5_{ox} quaternary structure in aqueous solution. Moreover, up to 500 mM NaCl had no effect on the sedimentation coefficient of HD5_{ox} at pH 7.0 (10 mM sodium phosphate buffer) (Table S10, Figure S30).

Using both the NMR solution structure and the X-ray crystal structure of HD5_{ox} as models, sedimentation coefficients were

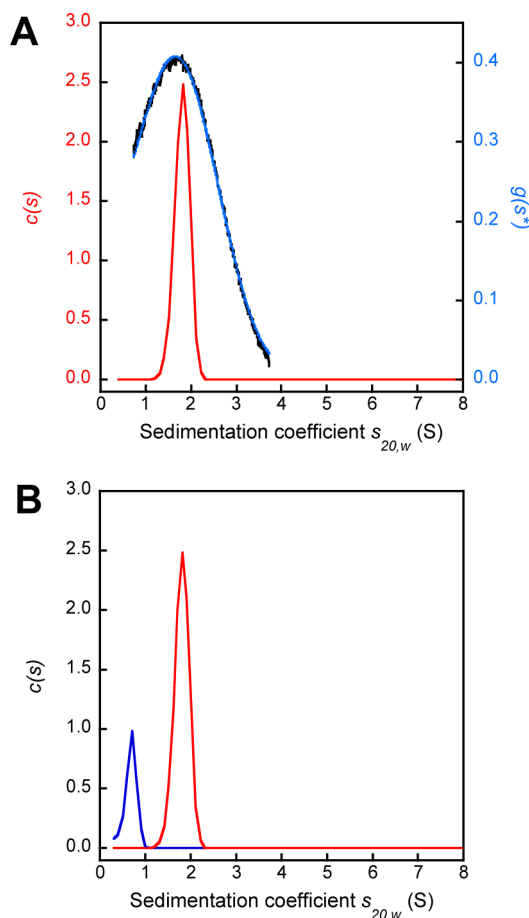


Figure 6. Sedimentation coefficient determination for HD5_{ox} and HD5[Ser^{hexa}] at pH 7.0 (10 mM sodium phosphate buffer) by analytical ultracentrifugation. (A) Sedimentation coefficient determination for 301 μ M HD5_{ox}. The black curve is the apparent sedimentation coefficient distribution $g(s^*)$. The blue curve is the single Gaussian fit of this data. The red curve is the diffusion-deconvoluted sedimentation coefficient distribution $c(s)$. These analyses provide a S -value of 1.8 S and indicate that HD5_{ox} is tetrameric under these experimental conditions. (B) Comparison of the diffusion-deconvoluted sedimentation coefficient distributions of 91 μ M HD5[Ser^{hexa}] (blue) and 301 μ M HD5_{ox} (red). Additional sedimentation velocity data for HD5_{ox} and mutant peptides are provided as Supporting Information.

estimated using HYDROPRO to be 0.66 S (monomer), 1.16 S (dimer), and 1.71 S (tetramer) (Table S3). The HD5_{ox} homodimer observed in the crystalline form was employed to calculate the dimer sedimentation coefficient. Two different models of HD5_{ox} tetramers were generated from the crystallographic structure and evaluated, and each provided the same predicted S -value. A comparison of the experimentally obtained and calculated S -values indicates that HD5_{ox} exists in a tetrameric form in aqueous buffer at neutral pH at concentrations $\geq 30 \mu$ M. Moreover, this comparison suggests that pH modulates HD5_{ox} quaternary structure and that dimers predominate at lower pH.

Equation 2 was employed to determine minimum frictional ratios (f/f_0) and thereby provide a semiquantitative analysis of maximum shape asymmetry for HD5_{ox}. In all cases, the f/f_0 ratio was ~ 1.2 , which suggests that the HD5 oligomers exhibit globular shape. No extended elongation is predicted for the tetrameric form.

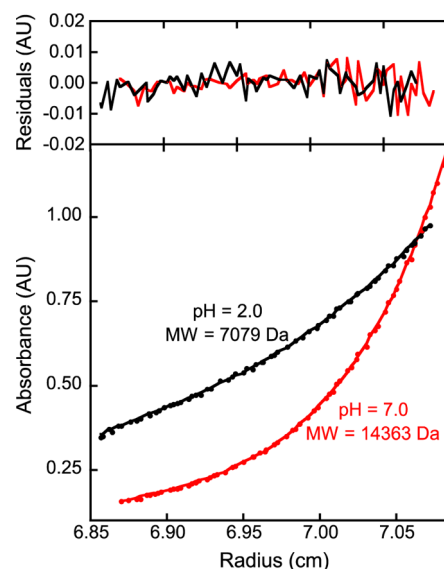


Figure 7. Sedimentation equilibrium of 189 μ M HD5_{ox} at pH 2 (black) and 187 μ M HD5_{ox} at pH 7 (red) in 10 mM sodium phosphate buffer. Top panel: The residuals of the fits. Bottom panel: Sedimentation equilibrium data (circles) and fits (lines) at a rotor speed of 36 000 rpm. Additional sedimentation equilibrium data for HD5_{ox} and mutant peptides are provided as Supporting Information.

Sedimentation Equilibrium Studies of HD5_{ox} Quaternary Structure. SE experiments were subsequently conducted to determine the molecular weight of the HD5_{ox} species observed to sediment at 1.8 S (Figures 7 and S31–S36). Samples of varying HD5_{ox} concentrations were used to collect absorbance equilibrium profiles at speeds appropriate for a ~ 14 kDa globular peptide (10 mM sodium phosphate buffer, pH 7.0). After global analysis of six different HD5_{ox} samples at pH 7.0, each at three different rotor speeds, the calculated molecular weight was determined to be 14 363 Da. This value is within 1% error of the theoretical molecular weight of a HD5_{ox} tetramer (14 328 Da). The globally fit value has a standard deviation of ± 32 Da and at the 95% confidence interval ranged from 14 472–14 716 Da using a Monte Carlo analysis of fit (Table S12). This analysis was extended to HD5_{ox} samples at varying pH, and the molecular weight calculations of samples prepared at pH values of 4.0, 6.0 and 8.0 also converged to tetrameric molecular weights; however, the global reduced chi-squared values increased with decreasing pH from 7.0 to 4.0. The data obtained at pH 4.0 could be fit using the molecular weight of a HD5_{ox} dimer, but the residuals of the fit were poor compared to those obtained after converging to a tetramer molecular weight (Figures S34 and S35). Moreover, a markedly different sedimentation profile of HD5_{ox} at pH 2.0 was observed and afforded a best-fit molecular weight of 7079 Da (Figure 7). This molecular weight corresponds to a dimer within 2% error (7164 Da). These results confirm that the HD5_{ox} oligomerization state in aqueous solution is pH-dependent with dimers predominating at relatively low pH and tetramers forming at higher pH values.

Sedimentation Velocity Studies of Disulfide Mutant Quaternary Structure. To evaluate the consequence of disulfide bond deletion on quaternary structure, SV experiments were performed with the regioisomers of HD5[Ser^{3,31}]_{ox} and HD5[Ser^{10,30}]_{ox} in addition to HD5[Ser^{hexa}]_{ox} at pH 7.0 (10 mM sodium phosphate buffer). Regardless of peptide

concentration and method of analysis (e.g., $c(s)$ and dc/dt), each peptide exhibited sedimentation coefficient values that were markedly and consistently lower than those of wild-type HD5_{ox} obtained under the same conditions (Table S5 and Figures S37–S39). The sedimentation coefficient values for the HD5[Ser^{3,31}]_{ox} and HD5[Ser^{10,30}]_{ox} regioisomers averaged ca. 0.80 S and ca. 0.90 S, respectively. These values fall between the HYDROPRO-calculated *S*-values for the HD5 dimer (1.16 S) and monomer (0.71 S). The hexa mutant sedimentation coefficient averaged ca. 0.67. These results demonstrate that loss of the Cys³–Cys³¹ or Cys¹⁰–Cys³⁰ disulfide bond, or linearization of the peptide backbone, prohibits tetramer formation at pH 7.0. Linearization affords a monomeric, random coil species. Loss of one disulfide bond results in one or more unfolded species that may be described as lower-order oligomers. HYDROPRO calculations of energy-minimized random coil structures of these disulfide deletion mutants also supported the presence of monomeric species.

DISCUSSION

In this work, we present the results of biophysical investigations designed to probe the solution structure and oligomerization properties of the human host-defense peptide HD5_{ox} and a family of disulfide deletion mutants. First, multidimensional NMR spectroscopy afforded the HD5_{ox} solution structure (Figure 4) and confirmed a dimeric oligomerization state under the NMR sample conditions. Second, analytical ultracentrifugation experiments conducted over a range of pH values and in the presence and absence of millimolar Na(I), Ca(II), and Mg(II) delineated factors that contribute to HD5_{ox} oligomerization in aqueous solution. One particularly noteworthy observation is the effects of buffer and pH on the formation and disassembly of HD5_{ox} tetramers (Figure 7). Lastly, complementary studies of disulfide array mutant peptides and HD5_{red} confirmed that the native α -defensin scaffold, defined by the tridisulfide array, is essential for structural rigidity and the formation of well-defined oligomeric species. Taken together, these studies afford insights into the solution behavior, oligomerization properties, and disulfide array of HD5_{ox}, which provide a basis for further understanding its biological activities and evaluating its structure and function in the context of other α -defensin family members.

All α -defensins share the same regiospecific pairing of cysteine residues (I–VI, II–IV, III–V, with Cys numbered sequentially from N- to C-terminus) and a three-stranded β -sheet fold. Other conserved features include an invariant Gly residue (Gly¹⁸ in HD5) and the Arg–Glu salt bridge. Nevertheless, the primary amino acid sequences and overall charges of α -defensins are variable, affording diverse structural dynamics and biological activities, and necessitating evaluation of α -defensin family members on a case-by-case basis.

Atomic-level solution structural characterization is important for elucidating structure/function relationships of antimicrobial peptides.⁷⁰ Comparison of the HD5_{ox} solution structure with other α -defensin structures reveals noteworthy similarities and differences. Crystallographic characterization of HD5_{ox} provided several different monomeric forms (PDB: 1ZMP).¹⁰ Overlay of the HD5_{ox} solution structure and the HD5_{ox} crystallographic monomers shows marked topological agreement and provides a RMSD of 1.042 Å for heavy backbone atoms (Figure S40). Likewise, the backbones of HD5_{ox} and HNP3 (PDB: 1DFN) are highly similar with a RMSD of 1.073 Å (Figure S41). The cysteine residues of HNP3 and HD5 share

primary amino acid sequence positions, and both peptides exhibit well-defined N- and C-termini in solution (Figure S41). Although HD5_{ox} shares the overall α -defensin fold of rabbit kidney-defensin RK-1⁷¹ and murine cryptdin-4,⁴³ the latter two peptides exhibit markedly increased conformational flexibility at the N- and C-termini that results from the positioning of the I and VI cysteine residues (Figure S41B). The biological ramifications of variable termini flexibility in α -defensins are currently unclear; however, studies of β -defensins indicated that termini flexibility may contribute to oligomerization.⁷²

The disulfide array imposes the α -defensin topology exhibited by HD5 and other family members, and also confers protease resistance. The NMR studies of the disulfide deletion mutants are in agreement with prior NMR characterization of cryptdin-4 disulfide array mutants⁴² and reduced HBD-1,⁶⁴ and further confirm that disulfide deletion results in a loss of peptide fold. Moreover, the ¹H,¹⁵N-HSQC spectra of mutants lacking a single disulfide bond indicate that multiple species are present in solution. Guided by the sedimentation coefficients obtained for the HD5[Ser^{3,31}]_{ox} and HD5[Ser^{10,30}]_{ox}, which fall between the calculated *S*-values of the HD5_{ox} monomer and dimer, we contend that the speciation may result from mixtures of oligomeric species.

Recent mutagenesis studies have highlighted the importance of both electrostatics and hydrophobicity in human α -defensin antibacterial action.^{4,35–37} Electrostatic and hydrophobicity depictions of select α -defensins are provided as Supporting Information (Figures S42–S47). The primary amino acid sequence of HD5 contains six arginine residues (Figure 1). Arg⁶ is involved in the salt-bridge, and the five remaining Arg residues are distributed along one side of the tertiary surface (Figure 4C). The opposite face contains a largely hydrophobic and slightly concave area. This region houses Val¹⁹, Ile²², and Leu²⁹ in addition to Cys³–Cys³¹ and Cys⁵–Cys²⁰. Only one charged residue, Glu²¹, is located on this face (Figure S43), and it is adjacent to the tight beta type-I turn. HD5_{ox} therefore exhibits amphipathic character. Many defensins are amphipathic in nature, and this attribute is generally accepted to be important for membrane interactions and antimicrobial activity.⁴ Nevertheless, the number and arrangement of Arg residues in α -defensins are variable, and HD5_{ox} exhibits a relatively well-defined cluster of Arg residues on one topological surface as compared to HNPs and cryptdin-4 (Figures S19 and S44). This feature is likely relevant to the HD5_{ox} mechanism(s) of antimicrobial action. Along such lines, replacement of select Arg residues with Ala or Lys attenuated the antibacterial activity of HD5_{ox} against several bacterial species.²⁸

The propensity of defensins to self-associate and form oligomers is considered to be important for various biological functions, including bacterial membrane disruption and antiviral activity.⁴ Nevertheless, few thorough investigations of defensin quaternary structure are in the literature, and how sample conditions contribute to the observed oligomerization states are largely unknown. Biophysical characterization of the θ -defensin retocyclin-2 exemplified the importance of buffer composition for oligomerization.⁷³ The first crystallographic characterization of an α -defensin revealed HNP3 in a dimeric form,⁶⁶ and this structural feature was hypothesized to be important for bacterial membrane permeabilization. Later solid-state NMR spectroscopic studies of HNP1 suggested a dimer pore mechanism of membrane disruption.⁷⁴ Recent investigations demonstrated the importance of HNP1 dimerization

in antibacterial activity, anthrax lethal factor inhibition, and binding to HIV-1 gp120.³⁷ A model of HNP1 tetramerization was also proposed in this work. Crystallographic characterization of other human α -defensins, including HD5 and HNP4, also revealed dimeric forms.¹⁰ Dimers of human β -defensin HBD-3⁷² and the plant defensin NaD1⁷⁵ have been observed in solution. In contrast, monomers of cryptdin-4,⁷⁶ RK-1,⁷¹ and human β -defensins⁷² HBD-1 and -2 were identified. Self-assembly of HD6 “nanonets,” or higher-order oligomers, was recently described and implicated in protection of the intestinal mucosa from bacterial invasion.⁷⁷ Taken together, these studies indicate that defensin oligomerization is highly variable and likely dependent on the sample conditions, making direct comparisons difficult and complicating predictions of oligomeric state.

The dimeric oligomerization state of HD5_{ox} in the NMR sample (90:10 H₂O/D₂O, pH 4.0) was first indicated by analysis of T_2 values and later confirmed by a ¹⁵N-TRACT experiment. Indeed, self-association of HD5_{ox} was observed by crystallography and surface plasmon resonance (SPR).^{10,35,78} A dissociation constant of ca. 2 μ M was obtained from SPR experiments conducted at pH 7.4 and in the presence of 150 mM NaCl, attributed to dimer formation; evidence for higher-order oligomers was reported at HD5_{ox} concentrations greater than ca. 8 μ M.⁷⁸ Recent mutagenesis studies indicated a hydrophobic mode of dimerization.³⁵ The structural studies presented in this work further confirm the importance of hydrophobicity in HD5_{ox} quaternary structure. The ¹³C-edited NOESY spectrum revealed a number of exchange-broadened $H\alpha$ signals, including those corresponding to residues Cys²⁰ and Glu²¹ housed on the outermost sheet of the β -bulge. Exchange broadening of $H\alpha$ signals was also observed for residues Thr⁷ and Cys¹⁰ of the loop. Exchange broadening was judged to occur at these positions because a lack of recordable data corresponding to these atoms was obtained in the ¹³C-edited NOESY spectrum. Lastly, the backbone ¹⁵N T_2 measurements indicate that specific regions of the peptide undergo conformer exchange broadening (Figure 5B). Asymmetric tumbling is an alternative explanation for the differential levels of T_2 relaxation because this phenomenon results in longer T_2 times away from the center of mass. HD5_{ox} is not a spherical molecule; however we contend that a spherical model for tumbling is sufficient, and differential tumbling along unequal axes does not account for the distribution of T_2 times measured (Figure S48). Residues 22–24 comprising the beta turn are the most distant from the center of mass. These residues exhibit some of the most ideal T_2 values (e.g., close to the $S^2 = 1.0$ line, Figure 5C). The order parameter plots exhibited in Figure 5C are based on the Lipari and Szabo ‘model free’ theory,^{68,69} which assumes spherical tumbling, and suggests that a spherical model for HD5_{ox} tumbling is appropriate for the beta turn residues. In contrast, short T_2 values are observed for many residues in loop 7–14. This loop also traces along points that are distant from the center of mass, and these T_2 values are inconsistent with asymmetric tumbling. We therefore conclude that the T_2 times in HD5_{ox} are indicative of a dimeric interface that is exchanging between free and bound forms on the millisecond time scale.

In contrast, the analytical ultracentrifugation studies presented in this work indicate that HD5_{ox} exists as a tetramer at >30 μ M in buffered aqueous solution at neutral pH (Figures 6 and 7). Taking the sedimentation equilibrium results into account, we speculate that the significant peak broadening and

heterogeneous signal intensities observed in the ¹H,¹⁵N-HSQC NMR spectra of ¹⁵N-HD5_{ox} prepared in buffered solutions resulted from tetramer formation. Further sedimentation velocity experiments indicated that the tetramer was unaffected by varying the sample concentration or buffer composition (phosphate vs Tris vs HEPES), or by addition of millimolar concentrations of the divalent cations Na(I), Ca(II) and Mg(II). We chose to investigate the consequences of cation addition because the antibacterial activity of HD5 is “salt-sensitive.” Like many defensins, addition of millimolar concentrations of NaCl to assay buffer results in attenuated antibacterial activity *in vitro*.²² This phenomenon is typically attributed to a salt-induced disruption of electrostatic interactions between the defensin and negatively charged bacterial cell surface. The results presented in this work demonstrate that up to 500 mM NaCl does not perturb HD5_{ox} quaternary structure over the peptide concentration range tested, suggesting that disrupted oligomerization does not contribute to attenuated antibacterial activity in the presence of salt. In contrast, the absence or presence of buffer and also pH modulate the HD5_{ox} oligomerization state. In phosphate buffer, HD5_{ox} oligomerization is influenced by pH. The pH effect is evidenced by the S -values obtained from the SV measurements and in the SE data (Figure 7). The conclusion that HD5_{ox} is best described as a dimer at pH 4.0 in unbuffered solution and as a tetramer in the presence of 10 mM sodium phosphate at pH 5.0 illustrates the importance of solution composition when evaluating defensin oligomerization states. Indeed, prior solution studies of retocyclin-2 revealed buffer-dependence.⁷³ A trimer was observed at pH 7.4 in either phosphate or Tris buffer whereas, in unbuffered solution, the trimer was only observed at higher peptide concentrations. Further investigations are required to elucidate the molecular basis for this pH-dependent self-association from dimer to tetramer in addition to residues that comprise the tetramer interface of HD5_{ox}.

HD5 is released from Paneth cells into the human small intestinal lumen where it contributes to mucosal immunity. Estimates for the extracellular concentration of Paneth cell defensins vary from 50–250 μ g/mL (luminal HD5)²¹ to ≥ 25 mg/mL (cryptdin-4 at the point of secretion).⁷⁹ The NMR and AUC studies presented in this work are in this concentration range. Moreover, the AUC investigations cover a pH range relevant to the small intestine in physiological and pathological states. This environment is relatively neutral to slightly alkaline environment under healthy conditions largely as a result of bicarbonate production by the pancreas and mucosa, and becomes more acidic during inflammation.⁸⁰ Although the compositions of aqueous buffer and the intestinal mucosa/lumen differ substantially, and various small molecules such as fatty acids present in the gut may influence oligomerization, the results from this investigation suggest that HD5 may exist as a tetramer in the healthy gut. Moreover, it is intriguing to speculate that alterations in HD5 oligomerization, and hence function, may occur as a result of pH fluctuations *in vivo*, e.g., during intestinal inflammation as a result of a more acidic environment.

We previously reported that deletion of a single disulfide bond in HD5_{ox} results in loss of antibacterial activity against *S. aureus*.¹² Taking the current peptide stability and biophysical investigations into account, we conclude that this attenuated activity results from disrupted peptide fold and quaternary structure. Identifying particular cellular targets of HD5_{ox} for a

variety of bacterial species and characterizing the HD5_{ox}/target interaction(s) are required to further elucidate precisely how HD5_{ox} contributes to innate immunity and human health.

■ ASSOCIATED CONTENT

■ Supporting Information

Tables S1–S12 and Figures S1–S48. This information is available free of charge via the Internet at <http://pubs.acs.org>.

■ AUTHOR INFORMATION

Corresponding Author

*E-mail: lnolan@mit.edu. Phone: 617-452-2495. Fax: 617-324-0505.

Funding

This work was supported by NIH Grant DP2OD007045 (E.M.N.) from the Office of the Director, National Institutes of Health and NIH Grant P01 GM047467 (G.W.) from the National Institute of General Medical Sciences. The FBML is supported by NIH Grant EB-002026 from the National Institute of Bio-Medical Imaging and Bioengineering of the NIH. The content is solely the responsibility of the authors and does not necessarily represent the official views of the National Institutes of Health. Support was also received from the Department of Chemistry at MIT (E.M.N.). NMR instrumentation housed in the MIT DCIF is maintained by funding from the National Science Foundation (CHE-9808061). The MIT Biophysical Instrumentation Facility for the Study of Complex Macromolecular Systems is supported by Grants NSF-0070319 and NIH GM68762.

Notes

The authors declare no competing financial interest.

■ ACKNOWLEDGMENTS

We thank Ms. Debby Pheasant for assistance with the AUC experimental setup, Dr. Robert Radford and Dr. Nozomi Ando for helpful discussions about AUC, and Dr. Tsyr-Yan (Dharma) Yu for assistance in the collection and analysis of the TRACT NMR data.

■ ABBREVIATIONS USED

AUC, analytical ultracentrifugation; CFU, colony forming unit; HD5, human α -defensin 5; HD5_{red}, reduced human α -defensin 5; HD5_{ox}, oxidized human α -defensin 5; HNP, human neutrophil peptide (an α -defensin); HSQC, heteronuclear single quantum coherence; IPTG, isopropyl- β -D-thiogalactopyranoside; LB, Luria Broth; NOESY, nuclear Overhauser effect spectroscopy; OD, optical density; SE, sedimentation equilibrium; SV, sedimentation velocity; TFA, trifluoroacetic acid; TOCSY, total correlation spectroscopy; TROSY, transverse relaxation optimized spectroscopy; TSB, trypticase soy broth

■ REFERENCES

- (1) Choi, K.-Y., Chow, L. N. Y., and Mookherjee, N. (2012) Cationic host defence peptides: Multifaceted role in immune modulation and inflammation. *J. Innate Immun.* 4, 361–370.
- (2) Hazlett, L., and Wu, M. (2011) Defensins in innate immunity. *Cell Tissue Res.* 343, 175–188.
- (3) Niyonsaba, F., Nagaoka, I., and Ogawa, H. (2006) Human defensins and cathelicidins in the skin: Beyond direct antimicrobial properties. *Crit. Rev. Immunol.* 26, 545–575.
- (4) Lehrer, R. I., and Lu, W. (2012) Alpha-defensins in human innate immunity. *Immunol. Rev.* 245, 84–112.

- (5) Klotman, M. E., and Chang, T. L. (2006) Defensins in innate antiviral immunity. *Nat. Rev. Immunol.* 6, 447–456.
- (6) Ganz, T. (2003) Defensins: Antimicrobial peptides of innate immunity. *Nat. Rev. Microbiol.* 3, 710–720.
- (7) Schneider, J. J., Unholzer, A., Schaller, M., Schäfer-Korting, M., and Korting, H. C. (2005) Human defensins. *J. Mol. Med.* 83, 587–595.
- (8) Pazgier, M., Li, X., Lu, W., and Lubkowski, J. (2007) Human defensins: Synthesis and structural properties. *Curr. Pharm. Des.* 13, 3096–3118.
- (9) Cunliffe, R. N. (2003) alpha-Defensins in the gastrointestinal tract. *Mol. Immunol.* 40, 463–467.
- (10) Szyk, A., Wu, Z., Tucker, K., Yang, D., Lu, W., and Lubkowski, J. (2006) Crystal structures of human alpha-defensins HNP4, HD5, and HD6. *Protein Sci.* 15, 2749–2760.
- (11) Rajabi, M., de Leeuw, E., Pazgier, M., Li, J., Lubkowski, J., and Lu, W. (2008) The conserved salt bridge in human alpha-defensin 5 is required for its precursor processing and proteolytic stability. *J. Biol. Chem.* 283, 21509–21518.
- (12) Wanniarachchi, Y. A., Kaczmarek, P., Wan, A., and Nolan, E. M. (2011) Human defensin 5 disulfide array mutants: Disulfide bond deletion attenuates antibacterial activity against *Staphylococcus aureus*. *Biochemistry* 50, 8005–8017.
- (13) Jones, D. E., and Bevins, C. L. (1992) Paneth cells of the human small intestine express an antimicrobial peptide gene. *J. Biol. Chem.* 267, 23216–23225.
- (14) Mallow, E. B., Harris, A., Salzman, N., Russell, J. P., DeBerardinis, R. J., Ruchelli, E., and Bevins, C. L. (1996) Human enteric defensins: Gene structure and developmental expression. *J. Biol. Chem.* 271, 4038–4045.
- (15) Porter, E. M., Liu, L., Oren, A., Anton, P. A., and Ganz, T. (1997) Localization of human intestinal defensin 5 in Paneth cell granules. *Infect. Immun.* 65, 2389–2395.
- (16) Wehkamp, J., Chu, H., Shen, B., Feathers, R. W., Kays, R. J., Lee, S. K., and Bevins, C. L. (2006) Paneth cell antimicrobial peptides: Topographical distribution and quantification in human gastrointestinal tissues. *FEBS Lett.* 580, 5344–5350.
- (17) Quayle, A. J., Porter, E. M., Nussbaum, A. A., Wang, Y. M., Brabec, C., Yip, K.-P., and Mok, S. C. (1998) Gene expression, immunolocalization, and secretion of human defensin-5 in human female reproductive tract. *Am. J. Pathol.* 152, 1247–1258.
- (18) Spencer, J. D., Hains, D. S., Porter, E., Bevins, C. L., DiRosario, J., Becknell, B., Wang, H., and Schwaderer, A. L. (2012) Human alpha defensin 5 expression in the human kidney and urinary tract. *PLoS One* 7, e31712.
- (19) Porter, E. M., Bevins, C. L., Ghosh, D., and Ganz, T. (2002) The multifaceted Paneth cell. *Cell. Mol. Life Sci.* 59, 156–170.
- (20) Cunliffe, R. N., Rose, F. R. A. J., Keyte, J., Abberley, L., Chan, W. C., and Mahida, Y. R. (2001) Human defensin 5 is stored in precursor form in normal Paneth cells and is expressed by some villous epithelial cells and by metaplastic Paneth cells in the colon in inflammatory bowel disease. *Gut* 48, 176–185.
- (21) Ghosh, D., Porter, E., Shen, B., Lee, S. K., Wilk, D., Drazba, J., Yadav, S. P., Crabb, J. W., Ganz, T., and Bevins, C. L. (2002) Paneth cell trypsin is the processing enzyme for human defensin-5. *Nat. Immunol.* 3, 583–590.
- (22) Porter, E. M., van Dam, E., Valore, E. V., and Ganz, T. (1997) Broad-spectrum antimicrobial activity of human intestinal defensin 5. *Infect. Immun.* 65, 2396–2401.
- (23) Ericksen, B., Wu, Z., Lu, W., and Lehrer, R. I. (2005) Antibacterial activity and specificity of the six human alpha-defensins. *Antimicrob. Agents Chemother.* 49, 269–275.
- (24) Salzman, N. H., Ghosh, D., Huttner, K. M., Paterson, Y., and Bevins, C. L. (2003) Protection against enteric salmonellosis in transgenic mice expressing a human intestinal defensin. *Nature* 422, 522–526.
- (25) Salzman, N. H., Hung, K., Haribhai, D., Chu, H., Karlsson-Sjöberg, J., Amir, E., Tegatz, P., Barman, M., Hayward, M., Eastwood, D., Stoel, M., Zhou, Y., Sodergren, E., Weinstock, G. M., Bevins, C. L.,

Williams, C. B., and Bos, N. A. (2010) Enteric defensins are essential regulators of intestinal microbial ecology. *Nat. Immunol.* 11, 76–83.

(26) Wehkamp, J., Salzman, N. H., Porter, E., Nuding, S., Weichenthal, M., Petras, R. E., Shen, B., Schaeffeler, E., Schwab, M., Linzmeier, R., Feathers, R. W., Chu, H., Lima, H., Jr., Fellermann, K., Ganz, T., Stange, E. F., and Bevins, C. L. (2005) Reduced Paneth cell alpha-defensins in ileal Crohn's disease. *Proc. Natl. Acad. Sci. U. S. A.* 102, 18129–18134.

(27) Shi, J. (2007) Defensins and Paneth cells in inflammatory bowel disease. *Inflamm. Bowel Dis.* 13, 1284–1292.

(28) de Leeuw, E., Rajabi, M., Zou, G. Z., Pazgier, M., and Lu, W. (2009) Selective arginines are important for the antibacterial activity and host cell interaction of human alpha-defensin 5. *FEBS Lett.* 583, 2507–2512.

(29) Seo, E.-j., Weibel, S., Wehkamp, J., and Oelschlaeger, T. A. (2012) Construction of recombinant E. coli Nissle 1917 (EcN) strains for the expression and secretion of defensins. *Int. J. Med. Microbiol.* 302, 276–287.

(30) Buck, C. B., Day, P. M., Thompson, C. D., Lubkowski, J., Lu, W., Lowy, D. R., and Schiller, J. T. (2006) Human alpha-defensins block papillomavirus infection. *Proc. Natl. Acad. Sci. U. S. A.* 103, 1516–1521.

(31) Smith, J. G., and Nemerow, G. R. (2008) Mechanism of adenovirus neutralization by human alpha-defensins. *Cell Host Microbe* 3, 11–19.

(32) Gounder, A. P., Wiens, M. E., Wilson, S. S., Lu, W., and Smith, J. G. (2012) Critical determinants of human alpha-defensin 5 activity against non-enveloped viruses. *J. Biol. Chem.* 287, 24554–24562.

(33) de Leeuw, E., Burks, S. R., Li, X., Kao, J. P. Y., and Lu, W. (2007) Structure-dependent functional properties of human defensin 5. *FEBS Lett.* 581, 515–520.

(34) Wei, G., de Leeuw, E., Pazgier, M., Yuan, W., Zou, G., Wang, J., Ericksen, B., Lu, W.-Y., Lehrer, R. I., and Lu, W. (2009) Through the looking glass, mechanistic insights from enantiomeric human defensins. *J. Biol. Chem.* 284, 29180–29192.

(35) Rajabi, M., Ericksen, B., Wu, X. J., de Leeuw, E., Zhao, L., Pazgier, M., and Lu, W. (2012) Functional determinants of human enteric alpha-defensin HD5: Crucial role for hydrophobicity at dimer interface. *J. Biol. Chem.* 287, 21615–21627.

(36) Wei, G., Pazgier, M., de Leeuw, E., Rajabi, M., Li, J., Zou, G., Jung, G., Yuan, W., Lu, W.-Y., Lehrer, R. I., and Lu, W. (2010) Trp-26 imparts functional versatility to human alpha-defensin HNP1. *J. Biol. Chem.* 285, 16275–16285.

(37) Pazgier, M., Wei, G., Ericksen, B., Jung, G., Wu, Z., de Leeuw, E., Yuan, W., Szmajnski, H., Lu, W.-Y., Lubkowski, J., Lehrer, R. I., and Lu, W. (2012) Sometimes It takes two to tango: Contributions of dimerization to functions of human alpha-defensin HNP1 peptide. *J. Biol. Chem.* 287, 8944–8953.

(38) Zhao, L., Ericksen, B., Wu, X., Zhan, C., Yuan, W., Li, X., Pazgier, M., and Lu, W. (2012) Invariant Gly residue is important for alpha-defensin folding, dimerization, and function: A case study of the human neutrophil alpha-defensin HNP1. *J. Biol. Chem.* 287, 18900–18912.

(39) Mandal, M., and Nagaraj, R. (2002) Antibacterial activities and conformations of synthetic alpha-defensin HNP-1 and analogs with one, two and three disulfide bridges. *J. Pept. Res.* 59, 95–104.

(40) Zou, G., de Leeuw, E., Li, C., Pazgier, M., Li, C., Zeng, P., Lu, W.-Y., Lubkowski, J., and Lu, W. (2007) Toward understanding the cationicity of defensins: Arg and Lys versus their noncoded analogs. *J. Biol. Chem.* 282, 19653–19665.

(41) Tanabe, H., Qu, X., Weeks, C. S., Cummings, J. E., Kolusheva, S., Walsh, K. B., Jelinek, R., Vanderlick, T. K., Selsted, M. E., and Ouellette, A. J. (2004) Structure-activity determinants in Paneth cell alpha-defensins: Loss-of-function in mouse cryptdin-4 by charge-reversal at arginine residue positions. *J. Biol. Chem.* 279, 11976–11983.

(42) Maemoto, A., Qu, X., Rosengren, K. J., Tanabe, H., Henschen-Edman, A., Craik, D. J., and Ouellette, A. J. (2004) Functional analysis of the alpha-defensin disulfide array in mouse cryptdin-4. *J. Biol. Chem.* 279, 44188–44196.

(43) Rosengren, K. J., Daly, N. L., Fornander, L. M., Jönsson, L. M. H., Shirafuji, Y., Qu, X., Vogel, H. J., Ouellette, A. J., and Craik, D. J. (2006) Structural and functional characterization of the conserved salt bridge in mammalian Paneth cell alpha-defensins: Solution structures of mouse cryptdin-4 and (E15D)-cryptdin-4. *J. Biol. Chem.* 281, 28068–28078.

(44) Hadjicharalambous, C., Sheynis, T., Jelinek, R., Shanahan, M. T., Ouellette, A. J., and Gizeli, E. (2008) Mechanisms of alpha-defensin bactericidal action: Comparative membrane disruption by cryptdin-4 and its disulfide-null analogue. *Biochemistry* 47, 12626–12634.

(45) Andersson, H. S., Figueredo, S. M., Haugaard-Kedström, L. M., Bengtsson, E., Daly, N. L., Qu, X., Craik, D. J., Ouellette, A. J., and Rosengren, K. J. (2012) The alpha-defensin salt bridge induces backbone stability to facilitate folding and confer proteolytic resistance. *Amino Acids* 43, 1471–1483.

(46) Masuda, K., Sakai, N., Nakamura, K., Yoshioka, S., and Ayabe, T. (2011) Bactericidal activity of mouse alpha-defensin cryptdin-4 predominantly affects noncommensal bacteria. *J. Innate Immun.* 3, 315–326.

(47) Studier, F. W. (2005) Protein production by auto-induction in high-density shaking cultures. *Protein Express. Purif.* 41, 207–234.

(48) Hyberts, S. G., Takeuchi, K., and Wagner, G. (2010) Poisson-gap sampling and FM reconstruction for enhancing resolution and sensitivity of protein NMR data. *J. Am. Chem. Soc.* 132, 2145–2147.

(49) Hyberts, S. G., Milbradt, A. G., Wagner, A. B., Arthanari, H., and Wagner, G. (2012) Application of iterative soft thresholding for fast reconstruction of NMR data non-uniformly sampled with multidimensional Poisson Gap scheduling. *J. Biomol. NMR* 52, 315–327.

(50) Delaglio, F., Grzesiek, S., Vuister, G. W., Zhu, G., Pfeifer, J., and Bax, A. (1995) NMRpipe: A multidimensional spectral processing system based on UNIX pipes. *J. Biomol. NMR* 6, 277–293.

(51) Goddard, T. D., Kneller, D. G. (2000) SPARKY 3, University of California, San Francisco.

(52) Keller, R. L. J. (2005) Optimizing the process of NMR spectrum analysis and computer aided resonance assignment. Thesis. ETH Zürich no. 15947. Swiss Federal Institute of Technology Zürich, Zürich, Switzerland.

(53) Cornilescu, G., Delaglio, F., and Bax, A. (1999) Protein backbone angle restraints from searching a database for chemical shift and sequence homology. *J. Biomol. NMR* 13, 289–302.

(54) Laskowski, R. A., MacArthur, M. W., Moss, D. S., and Thornton, J. M. (1993) PROCHECK: a program to check the stereochemical quality of protein structures. *J. App. Cryst.* 26, 283–291.

(55) Pettersen, E. F., Goddard, T. D., Huang, C. C., Couch, G. S., Greenblatt, D. M., Meng, E. C., and Ferrin, T. E. (2004) UCSF chimera - A visualization system for exploratory research and analysis. *J. Comput. Chem.* 25, 1605–1612.

(56) Koradi, R., Billeter, M., and Wüthrich, K. (1996) MOLMOL: A program for display and analysis of macromolecular structures. *J. Mol. Graphics* 14, 51–55.

(57) Laue, M., Shah, B. D., Ridgeway, T. M., and Pelletier, S. L. (1992) *Analytical Ultracentrifugation in Biochemistry and Polymer Science* (Harding, S.; Rowe, A., Eds.) pp 90–125, Royal Society of Chemistry.

(58) Lebowitz, J., Lewis, M. S., and Schuck, P. (2002) Modern analytical ultracentrifugation in protein science: A tutorial review. *Protein Sci.* 11, 2067–2079.

(59) Philo, J. S. (2000) A method for directly fitting the time derivative of sedimentation velocity data and an alternative algorithm for calculating sedimentation coefficient distribution functions. *Anal. Biochem.* 279, 151–163.

(60) Schuck, P. (2003) On the analysis of protein self-association by sedimentation velocity analytical ultracentrifugation. *Anal. Biochem.* 320, 104–124.

(61) Ortega, A., Amorós, D., and de la Torre, J. G. (2011) Prediction of hydrodynamic and other solution properties of rigid proteins from atomic- and residue-level models. *Biophys. J.* 101, 892–898.

(62) Schuck, P., and Braswell, E. H. (2000) Measurement of Protein Interactions by Equilibrium Ultracentrifugation, in *Current Protocols in*

- Immunology* (Coligan, J. E., Kruisbeek, A., Margulies, D. H., Shevach, E. M., Strober, W., Eds.), pp 18.18.11–18.18.22, Wiley, New York.
- (63) Vistica, J., Dam, J., Balbo, A., Yikilmaz, E., Mariuzza, R. A., Rouault, T. A., and Schuck, P. (2004) Sedimentation equilibrium analysis of protein interactions with global implicit mass conservation constraints and systematic noise decomposition. *Anal. Biochem.* 326, 234–256.
- (64) Schroeder, B. O., Wu, Z., Nuding, S., Groscurth, S., Marcinowski, M., Beisner, J., Buchner, J., Schaller, M., Stange, E. F., and Wehkamp, J. (2011) Reduction of disulphide bonds unmasks potent antimicrobial activity of human beta-defensin 1. *Nature* 469, 419–423.
- (65) Wüthrich, K. (1986) *NMR of Proteins and Nucleic Acids*, Wiley, New York.
- (66) Hill, C. P., Yee, J., Selsted, M. E., and Eisenberg, D. (1991) Crystal structure of defensin HNP-3, an amphiphilic dimer: Mechanisms of membrane permeabilization. *Science* 251, 1481–1485.
- (67) Lee, D., Hilty, C., Wider, G., and Wüthrich, K. (2006) Effective rotational correlation times of proteins from NMR relaxation interference. *J. Magn. Reson.* 178, 72–76.
- (68) Lipari, G., and Szabo, A. (1982) Model-free approach to the interpretation of nuclear magnetic resonance relaxation in macromolecules. 1. Theory and range of validity. *J. Am. Chem. Soc.* 104, 4546–4559.
- (69) Lipari, G., and Szabo, A. (1982) Model-free approach to the interpretation of nuclear magnetic resonance relaxation in macromolecules. 2. Analysis of experimental results. *J. Am. Chem. Soc.* 104, 4559–4570.
- (70) Bhattacharjya, S., and Ramamoorthy, A. (2009) Multifunctional host defense peptides: functional and mechanistic insights from NMR structures of potent antimicrobial peptides. *FEBS J.* 276, 6465–6473.
- (71) McManus, A. M., Dawson, N. F., Wade, J. D., Carrington, L. E., Winzor, D. J., and Craik, D. J. (2000) Three-dimensional structure of RK-1: A novel alpha-defensin peptide. *Biochemistry* 39, 15757–15764.
- (72) Schibli, D. J., Hunter, H. N., Aseyev, V., Starner, T. D., Wienczek, J. M., McCray, P. B., Jr., Tack, B. F., and Vogel, H. J. (2002) The solution structures of the human beta-defensins lead to a better understanding of the potent bactericidal activity of HBD3 against *Staphylococcus aureus*. *J. Biol. Chem.* 277, 8279–8289.
- (73) Daly, N. L., Chen, Y.-K., Rosengren, K. J., Marx, U. C., Phillips, M. L., Waring, A. J., Wang, W., Lehrer, R. I., and Craik, D. J. (2007) Retrocyclin-2: Structural analysis of a potent anti-HIV theta-defensin. *Biochemistry* 46, 9920–9928.
- (74) Zhang, Y., Lu, W., and Hong, M. (2010) The membrane-bound structure and topology of a human alpha-defensin indicate a dimer pore mechanism for membrane disruption. *Biochemistry* 49, 9770–9782.
- (75) Lay, F. T., Mills, G. D., Poon, I. K. H., Cowieson, N. P., Kirby, N., Baxter, A. A., van der Weerden, N. L., Dogovski, C., Perugini, M. A., Anderson, M. A., Kvensakul, M., and Hulett, M. D. (2012) Dimerization of plant defensin NaD1 enhances its antifungal activity. *J. Biol. Chem.* 287, 19961–19972.
- (76) Jing, W., Hunter, H. N., Tanabe, H., Ouellette, A. J., and Vogel, H. J. (2004) Solution structure of cryptdin-4, a mouse Paneth cell alpha-defensin. *Biochemistry* 43, 15759–15766.
- (77) Chu, H., Pazgier, M., Jung, G., Nuccio, S.-P., Castillo, P. A., de Jong, M. F., Winter, M. G., Winter, S. E., Wehkamp, J., Shen, B., Salzman, N. H., Underwood, M. A., Tsolis, R. M., Young, G. M., Lu, W., Lehrer, R. I., Bäuml, A. J., and Bevins, C. L. (2012) Human alpha-defensin 6 promotes mucosal innate immunity through self-assembled peptide nanonets. *Science* 337, 477–481.
- (78) Lehrer, R. I., Jung, G., Ruchala, P., Andre, S., Gabius, H. J., and Lu, W. (2009) Multivalent binding of carbohydrates by the human alpha-defensin, HD5. *J. Immunol.* 183, 480–490.
- (79) Ayabe, T., Satchell, D. P., Wilson, C. L., Parks, W. C., Selsted, M. E., and Ouellette, A. J. (2000) Secretion of microbicidal alpha-defensins by intestinal Paneth cells in response to bacteria. *Nat. Immunol.* 1, 113–118.
- (80) Nugent, S. G., Kumar, D., Rampton, D. S., and Evans, D. F. (2001) Intestinal luminal pH in inflammatory bowel disease: possible determinants and implications for therapy with aminosaclylates and other drugs. *Gut* 48, 571–577.
- (81) Grishaev, A., and Bax, A. (2004) An empirical backbone-backbone hydrogen-bonding potential in proteins and its applications to NMR structure refinement and validation. *J. Am. Chem. Soc.* 126, 7281–7292.